A Thermal Camera based Continuous Body Temperature Measurement System

Jia-Wei Lin, Ming-Hung Lu, Yuan-Hsiang Lin
Department of Electronic and Computer Engineering, Taiwan Building Technology Center
National Taiwan University of Science and Technology, Taipei, Taiwan
{m10702109, m10602107, linyh}@mail.ntust.edu.tw

Abstract

Body temperature acting an important role in medicine, a number of diseases are characterized by a change in human body temperature. Monitoring body temperature also allows the doctor to track the effectiveness of treatments. But current continuous body temperature measurement (CBTM) system is mainly limited by reaction time, movement noise, and labor requirement. In addition, the traditional contact body temperature measurement has the problem of wasting consumables and causing discomfort. To address above issues, we present a non-contact, automatic CBTM system using a single thermal camera. By applying deep-learning based face detection, object tracking, and calibrated conversion equation, we can successfully extract subject's forehead temperature in real-time. The experimental results show that the overall mean absolute error (MAE) and root-mean-squared-error (RMSE) of our proposed framework compared with industrial instrument are 0.375 ℃ and 0.439 ℃, respectively.

1. Introduction

Body temperature is one of the most important vital signs in human bodies. By monitoring the subject's body temperature, it is most directly known whether the patient has a fever or not, and even further can speculate on the effect of the treatment on the patient. It is especially important for users who need long-term monitoring (e.g., infants and the elderly). So now in hospitals, the body temperature is an indicator most commonly used by physicians to judge the subject's physiological conditions. Therefore, automated CBTM system has become a worldwide research issue, and the main goal is to measure body temperature accurately and for a long time.

As [1] mentioned, today's continuous body temperature measurement methods can be mainly divided into 2 types: the direct contact type and the non-contact type. The contact measurement method has the advantages of being unconstrained by the environment and having a wide temperature measurement range (about -90 °C to 300 °C). At present, most of the contact methods are used to measure body temperature (e.g., medical thermometers and thermistors), but this method not only requires labor, time and consumables, but also increases the workload of the care workers and causes a waste of resources. In addition, for the accuracy in the measurement process, the subject's activities will be limited, and the process may also cause discomfort. In contrast to the contact methods, non-contact body temperature measurement uses infrared (IR) techniques that do not require any contact with skin tissue during the procedure. Two types of infrared systems are mainly used, IR thermometers and thermal cameras. In this work, we chose the thermal camera to visualize the body temperature as an image, and measure the temperature at many points over a specific area.

This paper is organized as follows. In Section 2 presents the related work. In Section 3, we describe the proposed framework and our methods. In Section 4, the experiment and results are presented. Discussions and possible improvements for this work are drawn in Section 5. Finally, the conclusion is given in Section 6.

2. Related Work

Many papers on CBTM have been proposed today, while the main measurement methods are using non-invasive contact sensors. As W. Chen *et al.* introduced in [2], they use thermistors to monitor the baby's body temperature. However, when the user moves, the measured resistance will shift and cause temperature changes and errors. Also, it takes a long time to wait for the stable measurement reaction time, so the baby's body temperature cannot be known immediately. To improve the reaction time, the paper [3] proposed a multiple Artificial Neural Networks (ANNs) based wearable CBTM method to correct the thermistor, but the temperature will still be interfered by the user's movement. In 2018, NA. Livanos *et al.* proposed a handheld device using passive microwave radiometer (MWR) technology to measure the internal body temperature of a human body [4]. The device uses a non-contact measurement method to avoid user's movement artifacts. However, this device requires the user to aim at the part that he wants to measure, so the automatic measurement cannot be achieved.

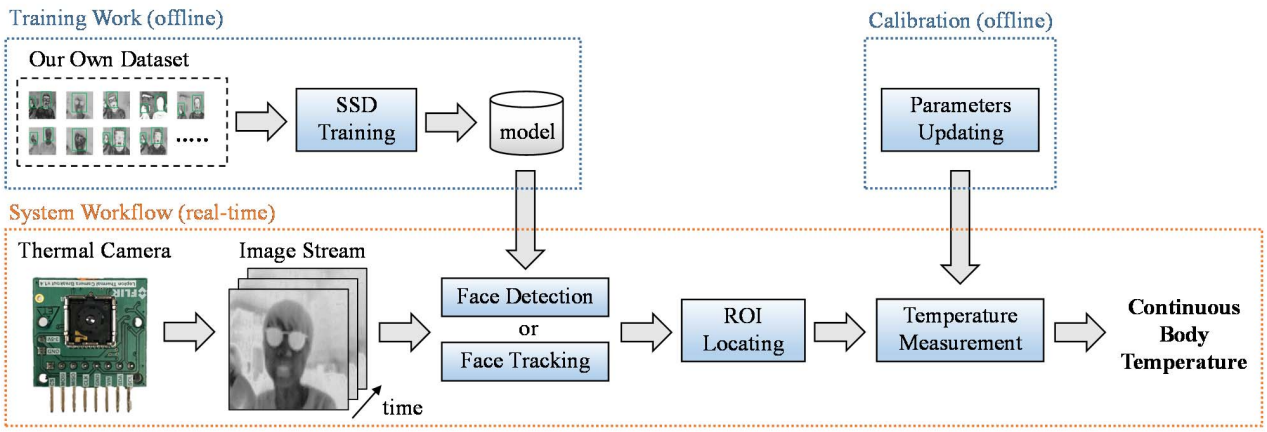

Figure 1. The proposed thermal camera-based continuous body temperature measurement framework.

Face detection is a very popular research topic in image processing, which has also been developed very maturely in the field of general full-color RGB cameras. On the other hand, to the best of our knowledge, there are currently three main methods for face detection in thermal images:

1) Image Projection method firstly convert thermal image to gray-scale image, and binarize the image by using the Ostu's method. After that, the vertical and horizontal projection of the binarized image is calculated, facial part can be defined from projection curve finally. In [5][6], this method has achieved good results and short processing time. However, it can only detect one face at a time.

2) Haar-Cascade method also known as Viola-Jones (VJ) method [7]. It can detect objects based on Haar-like features, Integral image, Adaptive Boosting (AdaBoost), and Cascade Classifier. This method has been successfully applied in several object detection applications such as face, animal, and vehicle detection. Authors of [8][9] used this algorithm to detect thermal face; however, the presented results indicated that the method was sensitive to the subject's head movement.

3) Machine Learning-based method was proposed in [10][11], the authors introduced a high-resolution thermal facial image database, which can be used to adapt methods from the visual domain for IR images. But unfortunately, the training images data of this database is too different from our camera specifications (our image has a poor-resolution while their database were recorded with 1024x768 pixel-sized). The application way are also dissimilar, so it is not suitable for this paper.

To sum up of the advantages and disadvantages of above papers, it can be observed that the current CBTM system is mainly limited by reaction time, movement noise and whether it can achieve automation. In this paper, we proposed a novel system according to these limitations. We used a thermal imaging sensor to build a non-contact CBTM system, and added the neural network-based face detection method and object tracking algorithm. After the thermal face detection is performed, the face is automatically tracked and the surface temperature in the region of interest (ROI) will be measured.

3. Methods

As the proposed framework illustrated in Figure 1, we adopt a FLIR Lepton 2.5 with breakout board to fetch sequential thermal images of subjects. FLIR Lepton 2.5 is a long-wave infrared (LWIR) camera sensor. It can capture infrared radiation input and output a uniform thermal image, where image size is 80x60 pixels, and thermal sensitivity is less than 50 mK (0.05 °C). The sensor's export compliant frame rate is around 9 Hz, video data can be accessed serially via the Serial Peripheral Interface (SPI) protocol.

Each frame is analyzed with the proposed framework. First of all, we use thermal face detection and tracking to locate the ROI in the facial part. Next, the raw value of body surface temperature is extracted from the determined ROI, and then pass through the calibrated formula to get the result. Our methods are constructed on the NVIDIA Jetson TX2 and written with C++ language and OpenCV library.

3.1. Thermal Face Detection

In this work, a good face detection is an important step for further processing. To achieve this goal, we decided to train a new model based on deep-learning method. Our method adopted the Single-Shot-Multibox Detector (SSD) [12] with MobileNet [13]. The MobileNet-SSD architecture is shown in Figure 2. One issue with deep-learning is the heavy demand for training data. To tackle this problem, we transferred the learned weights from pre-trained model [14], and fine-tuned it to our thermal images. This transferred learning process helped our detection model capture the features of thermal face with only a small dataset. The data used in our work came from a series of real-time execution,

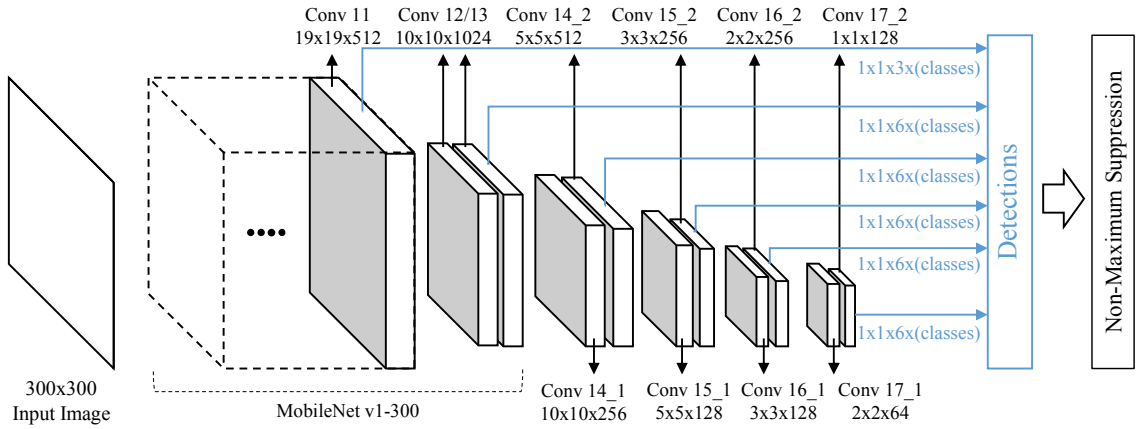

Figure 2. The overview of detection network architecture. Here, classes indicates the number of classes, which is 2 (thermal face and background) in this paper.

Figure 3. The result of deep-learning based thermal face detection.

which we sampled 1000 images in total. Among these images, 80% are used for training, 10% for validation, and 10% for testing. After 20000 iterations, our model had a loss rate of 0.169352. If any face is found, it returns the positions of detected faces as (1):

$$Face = Rect(x, y, w, h) \quad (1)$$

where x and y represent the coordinate of the top-left corner, w means width of the rectangle and h for height. Once we get these locations, we can easily draw a green rectangle for the face. Figure 3 shows the corresponding results of our thermal face detection.

3.2. Face Tracking

Although our deep-learning based face detection can accurately determine the location of the face in each frame, there is a disadvantage that the processing time is too long, leading to a decrease in frames per second (FPS). Therefore, we have added face tracking algorithm to improve the FPS in this system. Once the face is detected, kernel correlation filter (KCF) tracker [15] will be used to track the face region across each images. KCF is a highly accurate tracking algorithm. The general flow of the algorithm is as seen in Figure 4.

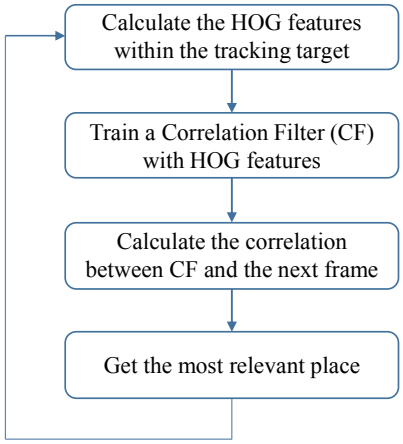

Figure 4. General flow of KCF algorithm.

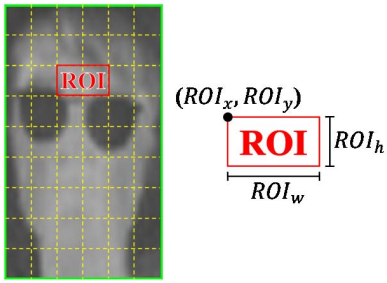

Figure 5. The illustration diagram of ROI assignment.

3.3. ROI Locating

After the face detection and tracking, we can determine the position of the subject's face in consecutively frames. For the subsequent measurement of body temperature, we use the face facial features to define the forehead area as our ROI (see Figure 5). The formula is defined as (2) and (3) below.

$$ROI = Rect\left(ROI_x, ROI_y, ROI_w, ROI_h\right) \tag{2}$$

$$\begin{cases} ROI_x = Face_x + 2 \times \dfrac{Face_w}{6} \\ ROI_y = Face_y + 2 \times \dfrac{Face_h}{9} \\ ROI_w = 2 \times \dfrac{Face_w}{6} \\ ROI_h = \dfrac{Face_h}{9} \end{cases} \tag{3}$$

3.4. Body Temperature Measurement

By referring the document [16], when radiometric mode is enabled, the 14-bit pixel value from Lepton is stabilized and normalized. A scene will correspond to a particular value in the video stream. The signal from the camera is called flux-linear because it is linear to the radiometric flux within Lepton's spectral band. The flux-linear signal is related to scene temperature by the Planck curve:

$$S = \int_{\lambda_1}^{\lambda_2} \frac{2\pi hc^2}{\lambda^5} \frac{1}{\exp(\frac{hc}{\lambda k T_k}) - 1} R(\lambda) \cdot \delta\lambda \tag{4}$$

where S is the output signal. λ_1 and λ_2 define the spectral band. h is Planck's constant. c is the velocity of light. k is Boltzmann's constant. $R(\lambda)$ is the camera responsivity. T_k is absolute temperature in units of Kelvin.

Since equation (4) is impractical to calculate in software, the conversion is typically approximated by equation (5):

$$S = \frac{R}{\exp\left(\frac{B}{T_k}\right) - F} + O \tag{5}$$

where S denotes the output signal from the camera. R, B, F, and O are parameters generated during calibration. T_k is the target's absolute temperature in units of Kelvin. The conversion from flux to temperature is performed using the inverse of equation (5). So we can express equation (5) as:

$$T_k = \frac{B}{\ln\left(\frac{R}{S - O} + F\right)} \tag{6}$$

3.5. Parameters Updating

In this paper, we can use the FLIR Lepton 2.5 camera sensor to get the thermal scene. However, the output of this camera is the unstabilized 14-bit pixel value instead of the actual temperature value. Therefore, in order to get accurate human body temperature, we must first perform the radiometry calibration on this sensor. According to the specification manual [16], we used the Keysight U5855A thermal imaging camera with temperature-variety water to correct the R, B, F, and O parameters used in equation (6).

Ideally, the heat source should be located at the distance similar to targets of interest in the applications. In this study, our system is measuring subjects at 40-80 cm to the camera. For the purpose of collecting data for curve-fitting, it is recommended to average the values in a ROI of the image. Typical expected ranges for R, B, F, and O parameters are revealed in [16], which are shown below:

$$\begin{aligned} R &= [10000, 1000000] \\ B &= [1200, 1700] \\ F &= [0.5, 3] \\ O &= [-16384, 16383] \end{aligned} \tag{7}$$

The F parameter is generally not varied from a value of 1 except for measuring a very high scene temperature outside of camera's valid range. The typical values for B parameter is 1428, which is given in the document. If F and B are fixed at the typical values, it is possible to calibrate the R (the camera responsivity) and O (the offset) by fitting the regression line. Figure 6 shows the output curve fitting with the nonlinear least squares (NLS) method. The calibrated value of R and O are 231159.5 and 6094.248, respectively. Finally, we can rewrite equation (6) to equation (8):

$$T = \frac{1428}{\ln\left(\frac{231159.5}{S - 6094.248} + 1\right)} - 273.15 \tag{8}$$

where T is our measured skin temperature in units of Celsius. S denotes the output signal from the thermal camera. Through equation (8), we can get the forehead temperature T (in units of Celsius) in each frame.

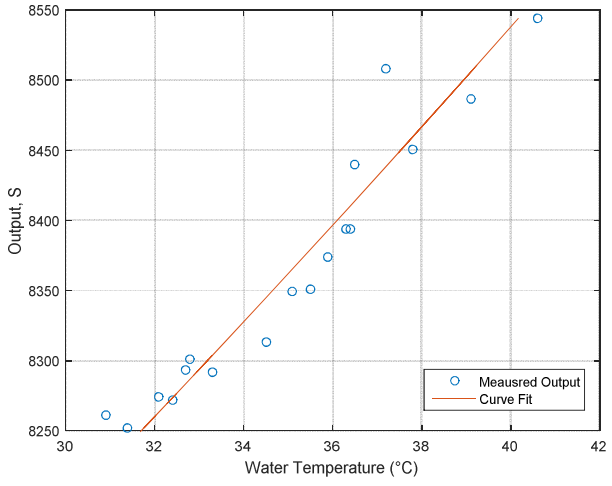

Figure 6. The fitting result of measured output.

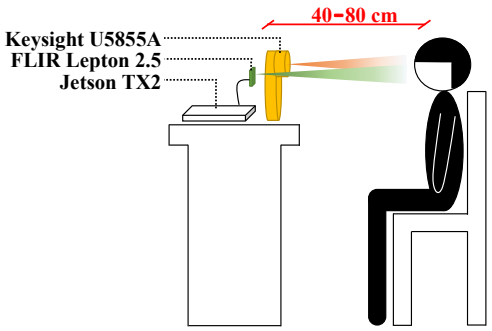

Figure 7. Illustration of the study setup.

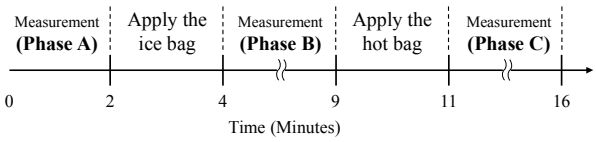

Figure 8. Experimental protocol.

4. Experiment and Results

4.1. Experimental Setup and Protocol

The experiment was conducted with 6 healthy subjects (4 males and 2 females). During the experiment, the FLIR thermal camera was set up 40-80 cm in front of the subjects to capture the sequential images at the speed of 26 FPS. All subjects were instructed to sit and maintain a stationary state. Furthermore, the Keysight U5855A camera was also placed to synchronize the ground-truth (GT) temperature at the maximum speed of 8 FPS. Figure 7 illustrates the measurement scenario.

In addition, the study protocol was carried out in a period of 16 minutes, which is represented in Figure 8. First, we measured the stable body temperature for two minutes (Phase A). Then, in order to simulate the change of body surface temperature, we put an ice bag and hot bag on the subject's forehead for two minutes, and then measured the body temperature change trend for five minutes, respectively (Phase B and C).

4.2. Experiment Results

In this paper, we adopted mean absolute error (MAE) and root-mean-squared-error (RMSE) metrics to express the difference between the proposed framework and the verified device. The operations are shown in (9) and (10). Table 1 shows the evaluation results provided by each subject.

$$\mathrm{MAE} = \frac{1}{N}\sum_{n=1}^{N}|T_n - REF_n| \tag{9}$$

$$\mathrm{RMSE} = \sqrt{\frac{1}{N}\sum_{n=1}^{N}(T_n - REF_n)^2} \tag{10}$$

where T_n is the average temperature of all pixel points in ROI. REF_n denotes the average temperature of similar area acquired from the GT device. These values are compared every 10 second. N refers to the number of obtained temperature within 10 second.

Finally, Figure 9 presents an example of the temperature estimated from our methods as well as the temperature corresponding to the GT. These representative signals are from subject 6.

Table 1. The results of the proposed CBTM system.

Subject	Phase A		Phase B		Phase C	
	MAE	RMSE	MAE	RMSE	MAE	RMSE
1	0.423	0.459	0.391	0.412	0.278	0.365
2	0.482	0.556	0.347	0.461	0.408	0.478
3	0.358	0.422	0.491	0.524	0.391	0.431
4	0.181	0.223	0.476	0.492	0.452	0.597
5	0.472	0.579	0.386	0.420	0.435	0.509
6	0.142	0.179	0.324	0.400	0.321	0.417
Average	**0.343**	**0.403**	**0.402**	**0.451**	**0.380**	**0.466**

※The unit of the values are Celsius (°C).

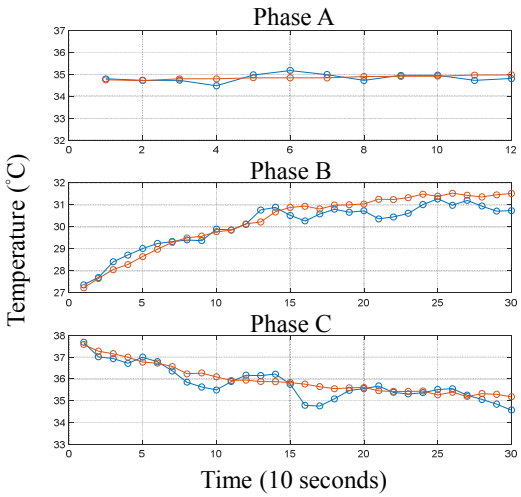

Figure 9. Representative example of the temperature of subject 6. The blue line indicates the temperature obtained from our system and the red line represents the ground-truth (GT).

5. Discussion

5.1. Face Detection

We have described a deep-learning approach to achieve this function. Although deep-learning based method requires more computing power and time than traditional image processing methods, it can overcome uncontrolled and complex environments in practical applications (i.e., in bedtime condition or some heat sources in background). On the issue of computing speed, we added a tracking method to improve the FPS of our system (from ~10 FPS to 26 FPS), the deep-learning based detection method will only be reused in the first frame or lost tracking. Therefore, we can fulfill the good detection accuracy and low execution time at the same time.

5.2. Experiment Methods

Our experimental results are compared with an industrial instrument. However, this limits our ability to only require the subject to remain stationary state during the experiment because it cannot track a specific area like our proposed system. For further experimentation, it is recommended to use an additional contact sensor such as medical thermometers or thermistors. In doing so, there may be a deviation between our non-contact method and contact method needs to be adjusted.

5.3. Future Work

In addition to body surface temperature, it is also possible to measure the core temperature of the human body. The scholars of the paper [17][18] used the body surface temperature (T_s), heat flow (HF), heart rate (HR) and other parameters to estimate the change of core temperature, which is also one of the main researches in the future.

Since thermal images have many advantages, such as unaffected by illumination variation, working well in darkness, and hard to fake than visible images, they are widely used in biometric applications. In the future, we can combine thermal face recognition and vital signs (i.e., pulse rate and respiration rate) monitoring under daily life.

6. Conclusions

In this paper, we developed a real-time, and contactless CBTM system with a low-cost and poor-resolution LWIR camera. To locate the subject's face, we trained a new model based on deep-learning method with our own dataset. We also applied a tracking algorithm to track detected face. Further, the immediate forehead temperature is obtained by the calibrated conversion formula. The experiment for the proposed framework shows that our system's overall mean absolute error (MAE) and root-mean-squared-error (RMSE) are 0.375 °C and 0.439 °C.

Acknowledgment

This work was supported in part by a research grant from the Ministry of Science and Technology under Grant MOST 107-2221-E-011-107- and financially supported by the Taiwan Building Technology Center from The Featured Areas Research Center Program within the framework of the Higher Education Sprout Project by the Ministry of Education in Taiwan.

References

[1] N. Sellier, E. Guettier, and C. Staub. A review of methods to measure animal body temperature in precision farming. *American Journal of Agricultural Science and Technology*, 2(2):74-99, 2014.

[2] W. Chen, S. Dols, S. B. Oetomo, and L. Feijs. Monitoring body temperature of newborn infants at neonatal intensive care units using wearable sensors. In *Proceedings of the IEEE 5th International Conference on Body Area Networks (BodyNets)*, pages 188-194, 2010.

[3] C. Song, P. Zeng, Z. Wang, H. Zhao, and H. Yu. Wearable continuous body temperature measurement using multiple artificial neural networks. *IEEE Transactions on Industrial Informatics*, 14(10):4395-4406, 2018.

[4] NA. Livanos *et al*. Design and interdisciplinary simulations of a hand-held device for internal-body temperature sensing using microwave radiometry. *IEEE Sensors Journal*, 18(6):2421-2433, 2018.

[5] J. Mekyska, V. Espinosa-Duró, and M. Faundez-Zanuy. Face segmentation: a comparison between visible and thermal images. In *IEEE International Carnahan Conference on Security Technology (ICCST)*, pages 185-189, 2010.

[6] Y. K. Cheong, V. V. Yap, and H. Nisar. A novel face detection algorithm using thermal imaging. In *IEEE Symposium on Computer Applications and Industrial Electronics (ISCAIE)*, pages 208-213, 2014.

[7] P. Viola, and M. Jones. Rapid object detection using a boosted cascade of simple features. In *Proceedings of the 2001 IEEE Computer Society Conference on Computer Vision and Pattern Recognition (CVPR), 2001*.

[8] A. Kwaśniewska, and J. Ruminski. Face detection in image sequences using a portable thermal camera. In *Proceedings of the 13th Quantitative Infrared Thermography Conference*, pages 4-8, 2016.

[9] A. Kwaśniewska, and J. Ruminski. Real-time facial feature tracking in poor quality thermal imagery. In *IEEE 9th International Conference on Human System Interaction (HSI)*, pages 504-510, 2016.

[10] M. Kopaczka, R. Kolk, and D. Merhof. A fully annotated thermal face database and its application for thermal facial expression recognition. In *IEEE International Instrumentation and Measurement Technology Conference (I2MTC)*, 2018.

[11] M. Kopaczka *et al*. A combined modular system for face detection, head pose estimation, face tracking and emotion recognition in thermal infrared images. In *IEEE International Conference on Imaging Systems and Techniques (IST)*, 2018.

[12] W. Liu, D. Anguelov, D. Erhan, C. Szegedy, and S. Reed. SSD: single shot multibox detector. *arXiv: 1512.02325*, 2015.

[13] AG. Howard *et al*. MobileNets: efficient convolutional neural networks for mobile vision applications. *arXiv: 1704.04861*, 2017.
[14] MobileNet-SSD. GitHub repository, [Online]. Available: https://github.com/chuanqi305/MobileNet-SSD/.
[15] J. F. Henriques, R. Caseiro, P. Martins, and J. Batista. High-speed tracking with kernelized correlation filters. *arXiv: 1404.7584*, 2014.
[16] FLIR. Lepton radiometry application note. Datasheet, 2014.
[17] X. Xu, AJ. Karis, MJ. Buller, and WR. Santee. Relationship between core temperature, skin temperature, and heat flux during exercise in heat. *Eur J Appl Physiol*, 113:2381-2389, 2013.
[18] AP. Welles *et al*. Estimation of core body temperature from skin temperature, heat flux, and heart rate using a kalman filter. *Computers in Biology and Medicine*, 99:1-6, 2018.